



Adsorptive removal of Congo red by surfactant modified cellulose nanocrystals: a kinetic, equilibrium, and mechanistic investigation

Damoon Ranjbar · Milad Raeiszadeh · Lev Lewis · Mark J. MacLachlan · Savvas G. Hatzikiriakos

Received: 11 August 2019 / Accepted: 24 January 2020
© Springer Nature B.V. 2020

Abstract A cellulose nanocrystal (CNC) based adsorbent was synthesized by modifying pristine CNC with various amounts of a positively-charged surfactant (CTAB) and was used to study the adsorption behavior of Congo red (CR) in aqueous medium. The interaction of CTAB with CNCs, and potential alterations on the chemical and physical structure of CNCs are studied, and the synthesized adsorbent, modified cellulose nanocrystal (MCNC) was characterized using Fourier transform infrared spectroscopy, X-ray diffraction, scanning electron microscopy, elemental and zeta potential analysis. The amount of surfactant used for modification was optimized to maximize the adsorption capacity of the adsorbent. Furthermore, it was found that the amount of surfactant affects the CR-MCNC interactions and determines the mechanism of adsorption. The kinetics followed a pseudo-second order and intra-particle

diffusion model implying that the rate-controlling step of the adsorption process was first dominated by film-diffusion, and consequently by intra-particle diffusion. Thermodynamic studies on the system suggested that the adsorption process is spontaneous and exothermic. Characterization of the adsorbent, before and after adsorption, coupled with the kinetic and isotherm studies indicated that electrostatic attraction, hydrogen bonding, and hydrophobic attraction are the main mechanisms/interactions of adsorption. The adsorbent is highly stable in water and retains its original adsorption capacity after successive dialysis cycles.

Keywords Cellulose nanocrystal · Surfactant · Adsorption · Congo red · Equilibrium

Electronic supplementary material The online version of this article (<https://doi.org/10.1007/s10570-020-03021-z>) contains supplementary material, which is available to authorized users.

D. Ranjbar · M. Raeiszadeh · S. G. Hatzikiriakos (✉)
Department of Chemical and Biological Engineering, The University of British Columbia, 2360 East Mall,
Vancouver, BC V6T 1Z3, Canada
e-mail: savvas.hatzi@ubc.ca

L. Lewis · M. J. MacLachlan
Department of Chemistry, University of British Columbia,
2036 Main Mall, Vancouver, BC V6T 1Z1, Canada

Introduction

Dyes and pigments are extensively used in the textile, leather, pharmaceutical, food, and cosmetic industries (Marco-brown et al. 2018). The continued discharge of wastewater containing dyes into the environment may have adverse effects on human health and the environment due to their toxicity, potential carcinogenicity, and mutagenicity (Zhou et al. 2014; Gao et al. 2019). High stability and solubility as well as non-biodegradability of industrial dyes have raised the need for adequate and effective treatment of the

wastewater before it enters the environment (Ding et al. 2018). Various biological and physicochemical methods have been developed for the treatment of contaminated wastewater, including photocatalysis (Dashtian et al. 2018), catalytic degradation (Rajeswari et al. 2017), chemical oxidation (Boczkaj and Fernandes 2017), membrane filtration (Wang et al. 2018a), and adsorption (Raeiszadeh et al. 2018). Among these methods, adsorption has been considered as the most beneficial due to its high efficiency, low cost, production of fewer byproducts, and simplicity of operation. Various classes of materials including hydrogels (Khan and Lo 2016), modified clay (Olusegun et al. 2018), graphene composites (Shu et al. 2017), and cellulosic extracts (Zhu et al. 2016) have been developed and examined for the adsorption of industrial dyes from wastewater. Despite great progress in this field, it is necessary to develop novel dye adsorbents in order to overcome the limitations of existing materials such as low adsorption capacity and complexity of synthesis.

Cellulosic materials continue to be promising candidates for dye adsorption mainly owing to their abundance, versatility, biodegradability, and environmental friendliness (Pan et al. 2016; Lin et al. 2017; Zhang et al. 2018). Furthermore, the existence of glucopyranose and three hydroxyl groups on each hydroglucose unit not only provides active sites for the adsorption of dye molecules, but it also makes various modifications and functionalization feasible to improve the dye removal properties of cellulose (Qiao et al. 2015). In the native cellulose fiber, the cellulose chains form an interconnected network due to the intermolecular hydrogen bonds resulting in the formation of substructures called microfibrils (Shafiei Sabet 2013). These microfibrils are composed of amorphous and crystalline regions, with the amorphous regions having lower density, aspect ratio, and surface area compared to the crystalline regions (Domingues et al. 2014). Chemical, mechanical and enzymatic treatments have been employed to release the highly crystalline regions of microfibrils, known as cellulose nanocrystals (CNCs) (Abdul Khalil et al. 2014). Among these methods, sulfuric acid hydrolysis has been found to produce CNCs that have high surface area and aspect ratio, hydrophilicity, broad functionalization capacity, chirality, and mechanical strength (Habibi et al. 2010; Lin et al. 2012; Kargazadeh et al. 2018; Ranjbar and Hatzikiriakos

2020). Furthermore, the presence of sulfate half-ester groups results in a high negative charge density on the surface of CNCs, making them dispersible in aqueous medium (Zhong et al. 2012). These unique properties have promoted CNCs as promising materials for the adsorption of industrial dyes. Since the presence of negative charges on the surface of CNCs facilitates the adsorption of cationic dyes, early studies on the adsorption properties of CNCs were mainly focused on cationic dyes (Batmaz et al. 2014). Moreover, various functionalization methods were used to improve the adsorption capacity of CNCs (Qiao et al. 2015). However, the unique features of CNCs attracted researchers to employ these nanoparticles in the adsorption process of anionic dyes as well. In several studies, CNCs were incorporated in the structure of a composite material to improve its dye adsorption properties. These composite materials include microgels (Jin et al. 2015b), polymeric ionic liquids (Beyki et al. 2016), and thin-film composite membranes (Bai et al. 2019). On the other hand, CNCs were adapted to the adsorption of anionic dyes by functionalization of their surface, such as with amino groups, which could improve their adsorption abilities (Jin et al. 2015a). Nevertheless, to the best of our knowledge, there have been no more studies, except the above mentioned, conducted on the adaptation of CNCs to the adsorption of anionic dyes by functionalization of its surface chemistry. Therefore, further research is required to gain a better understanding of the potential use of CNCs as adsorbents of anionic dyes.

Among the potential materials for functionalization purposes, surfactants have always been of great interest due to their hydrophilic-hydrophobic nature which sets the stage for their interaction with a wide variety of molecules and functional groups (Ding et al. 2018). Another unique property of surfactants is their ability to form bundles of surface-bound micelles, known as admicelles, on the colloidal particles in aqueous environments which could affect the interparticle interactions and induce distinctive features to the colloidal particles (Notley 2009; Khanari et al. 2011). In the past, surfactants have been used in several studies to improve the adsorption abilities of existing dye adsorbents. These studies include the modification of montmorillonite by several cationic surfactants (Wang and Wang 2008), hectorite with CTAB and octadecylamine (ODA) (Xia et al. 2011),

and the synthesis of organovermiculite-based adsorbent using CTAB (Yu et al. 2010). Nevertheless, there are no investigations performed on the potential contribution of surfactants to the anionic dye adsorption of CNCs.

Recently, the effect of a positive surfactant, CTAB, was investigated on the stability and dispersibility of CNC suspensions (Kaboorani and Riedl 2015). The advantages of using CTAB over other substances for the anionic dye adsorption using CNCs include its biodegradability by suitable micro-organisms (Zeng et al. 2007), low cost, and wide availability. In this study, the same method of modification is used on CNCs (Kaboorani and Riedl 2015). However, a detailed investigation was performed on surfactant-CNC complexes, and the interactions between modified CNCs (MCNCs). The contribution of CTAB to the anionic dye adsorption ability of MCNC, and the optimum conditions of modification are explored. Furthermore, the adsorption behavior of Congo red (CR) onto MCNC, including adsorption kinetics, isotherms, thermodynamics, and adsorption mechanisms are discussed. Finally, the stability of MCNC in aqueous environments and the regeneration of the adsorbent are investigated.

Experimental

Materials

Cellulose nanocrystals (CNCs) were purchased from CelluForce Inc. (Montreal, Quebec, Canada) in the form of spray dried sodium salts with sulfur content of 0.89 wt%, particle size of 1–50 μm (powder), and average hydrodynamic diameter of 70 nm, as reported by the supplier. Cetyltrimethylammonium bromide (CTAB) was purchased from Sigma-Aldrich with 98% purity. Congo red (CR) dye was purchased from Sigma-Aldrich, and dye solutions were prepared using deionized water.

Preparation of modified CNCs (MCNCs)

CNC suspensions of 5 wt% were prepared by dispersing CNC powder in deionized water. The suspension was stirred for 5 h followed by sonication. The amount of ultrasonic energy applied to the suspension was 10,000 J/g CNC powder (Shafiei-Sabet et al. 2012).

For the preparation of the CTAB solution, 5 g of CTAB powder was added progressively to a 100 mL beaker containing 95 g of deionized water which was being stirred on a hotplate inside a 50 °C bath. The stirring continued for roughly 30 min until the CTAB powder was fully dissolved and the solution stabilized.

In the preparation of modified CNCs (MCNCs), 40 g of the prepared 5 wt% CNC suspension was added to a 100 mL beaker while being stirred at 600 rpm. Subsequently varying amounts (ranging from 0.4 to 40 mL) of the prepared CTAB solution, depending on the desired weight fraction of CTAB/CNC, were added slowly to the beaker. The suspension was stirred for 2 h and centrifuged to obtain the modified CNC particles. To ascertain that no additional quaternary ammonium salts remained on the surface of CNC particles, they were thoroughly washed with DI water and filtered up to 10 times, as needed, using grade 50 Whatman filter paper, each followed by centrifugation at 12,000 rpm for 15 min. The obtained precipitates were collected and freeze dried under vacuum for 48 h. The final product was ground using a mortar and pestle and sieved through a mesh (number 50, 297- μm) to yield a fine dry powder.

CNC modification was conducted using various amounts of CTAB to investigate the effect of surfactant on the physical, chemical and dye adsorption characteristics of modified CNC. Eight different amounts of surfactant solution were added to the CNC suspension. These amounts are expressed as the weight ratio of CTAB to CNC, namely 0.01/1, 0.05/1, 0.1/1, 0.125/1, 0.25/1, 0.35/1, 0.65/1, and 1/1 w/w. These concentrations were chosen based on preliminary trial experiments to form adsorbents that exhibit both positive and negative surface charges. Each sample is identified by MCNC followed by a number showing the weight fraction of CTAB/CNC used in its modification. For example, MCNC 0.25 is the modified CNC sample in which the weight fraction of CTAB/CNC is 0.25 w/w.

Characterization of samples

Fourier transform infrared (FTIR) analysis

Fourier transform infrared (FTIR) analysis was performed to examine changes in the surface chemistry of CNCs, and the interactions between the dye molecules and adsorbents. FTIR spectra for pristine CNCs and

treated CNCs before and after adsorption were obtained using a PerkinElmer Frontier FT-IR in the range of 650–4000 cm^{-1} with a resolution of 4 cm^{-1} .

X-ray diffraction (XRD)

Since the crystalline structure plays a prominent role in the reinforcing effects of CNC particles, X-ray diffraction was used to investigate the possible alterations in the crystalline structure of CNCs as a result of modification with CTAB. Furthermore, the XRD patterns would detect the existence of any remaining undesirable quaternary ammonium salts during the synthesis process. X-ray diffraction was performed on unmodified and modified CNCs with different weight fractions of CTAB using a Bruker D8 Advance diffractometer.

Scanning electron microscopy (SEM)

Scanning electron microscopy was conducted using a Hitachi S4700 field-emission SEM to investigate the effect of modification on the morphology of CNC particles, and the possible effect of morphology on the adsorption of CR.

Elemental analysis

Elemental analysis was performed using a Thermo Flash 2000 Elemental analyzer to measure the sulfur and nitrogen content of MCNCs and obtain the S/N ratio (Sulfur from CNCs/Nitrogen from CTA^+) in order to investigate the dominance of these elements in MCNCs, with different amounts of CTAB, and explore their effect on the adsorption of CR.

Zeta potential measurement

Zeta potential measurement was conducted to investigate the effect of modification on the surface charge of CNC particles. 10 mg of the modified CNC samples were dispersed in 50 mL DI water and stirred for 1 h to obtain 0.02 wt% suspensions, similar to the dosage used for dye adsorption experiments. The zeta potential was measured using a Brookhaven NanoBrook Omni zeta potential analyzer. Each measurement was conducted 10 times over 50 cycles, and all the reported values are the average of 10 measurements. Since the

error bars were smaller than the symbol sizes, they are not included in the graphs to maintain clarity.

Dye adsorption experiments

Adsorption experiments were conducted at room temperature by adding 10 mg of MCNCs adsorbent to 50 mL of a Congo red (CR) dye solution (specific concentrations differ depending on the test specified in each case below) while being stirred at 600 rpm in a 100 mL beaker. The suspension was stirred for varying amounts of time between 5 and 120 min. The suspension was then centrifuged at 8000 rpm for 15 min. After removing the adsorbent, the residual concentration of CR in the solution was determined by measuring the maximum absorption intensity (at 600 nm for CR) using a Cary 100 UV-Vis spectrophotometer. The measured intensities were converted to concentration (mg L^{-1}) using the calibration curve of CR dye obtained through serial dilution of CR solutions over the range 1 to 400 mg L^{-1} . The dye adsorption capacity of the adsorbents at contact time, t min, was calculated using the following equation:

$$q_t = \frac{(C_0 - C_t)V}{m} \quad (1)$$

where C_0 (mg L^{-1}) is the initial dye concentration in the solution, C_t (mg L^{-1}) is the concentration of dye in the solution at time t , V (L) is the volume of the dye solution, and m (g) is the mass of adsorbent added to the dye solution.

The percentage of removal was calculated by:

$$\text{Removal}\% = \frac{(C_0 - C_t)}{C_0} \times 100 \quad (2)$$

And the equilibrium adsorption capacity was calculated using:

$$q_e = \frac{(C_0 - C_e)V}{m} \quad (3)$$

where C_e (mg L^{-1}) is the concentration of dye solution at equilibrium.

To study the kinetics of adsorption, a new dye solution was prepared for each contact time, and the concentration of CR was fixed to 100 mg L^{-1} in all experiments. Furthermore, the isotherm

study was conducted over a dye concentration range of 50 to 400 mg L^{-1} . All adsorption experiments were

performed three times and the reported results are the average of three replicates.

Regeneration study

The dye-loaded MCNCs were removed from the dye solution, after being agitated in 100 mg L^{-1} CR solution until equilibrium was reached, by centrifugation. These dye-loaded MCNCs were then introduced into a beaker containing 200 mL of 100% ethanol and stirred for 12 h at $25 \text{ }^\circ\text{C}$ with stirring speed of 100 rpm. After the desorption, MCNCs were washed and filtered following the same protocol as elaborated in the synthesis section and were used for the next cycles. A total of 5 successive adsorption–desorption cycles were performed on the adsorbent.

Results and discussion

FTIR analysis

The FTIR spectra of modified CNCs (MCNCs) are depicted in Fig. 1. After modification new peaks

appear at $2917\text{--}2919$ and $2850\text{--}2851 \text{ cm}^{-1}$, which are assigned to C–H stretching bands of the $-\text{CH}_3$ and $-\text{CH}_2$ groups of CTAB, respectively (Kaboorani and Riedl 2015). Furthermore, these peaks intensify considerably as the weight fraction of CTAB increases to 0.125 (Fig. S1). In addition, a weak intensity peak associated with $-\text{CH}_2$ bending and methyl groups was observed at $1430\text{--}1460 \text{ cm}^{-1}$, at higher concentrations of CTAB, which could be attributed to the cationic surfactant (Zaman et al. 2012). The FTIR spectra for the rest of the MCNC samples can be found in the supplementary information (Fig. S1).

Figure 2 shows the FTIR spectrum of MCNC 0.25 before and after the adsorption process. Intense and apparent peaks were observed at 662 and 831 cm^{-1} , associated with the C=C bending vibrations, and 1610 cm^{-1} , associated with the C=C stretching, which corresponds to the phenyl groups in the structure of the CR dye (Wang et al. 2016). These results confirm the successful adsorption of CR by the synthesized adsorbents.

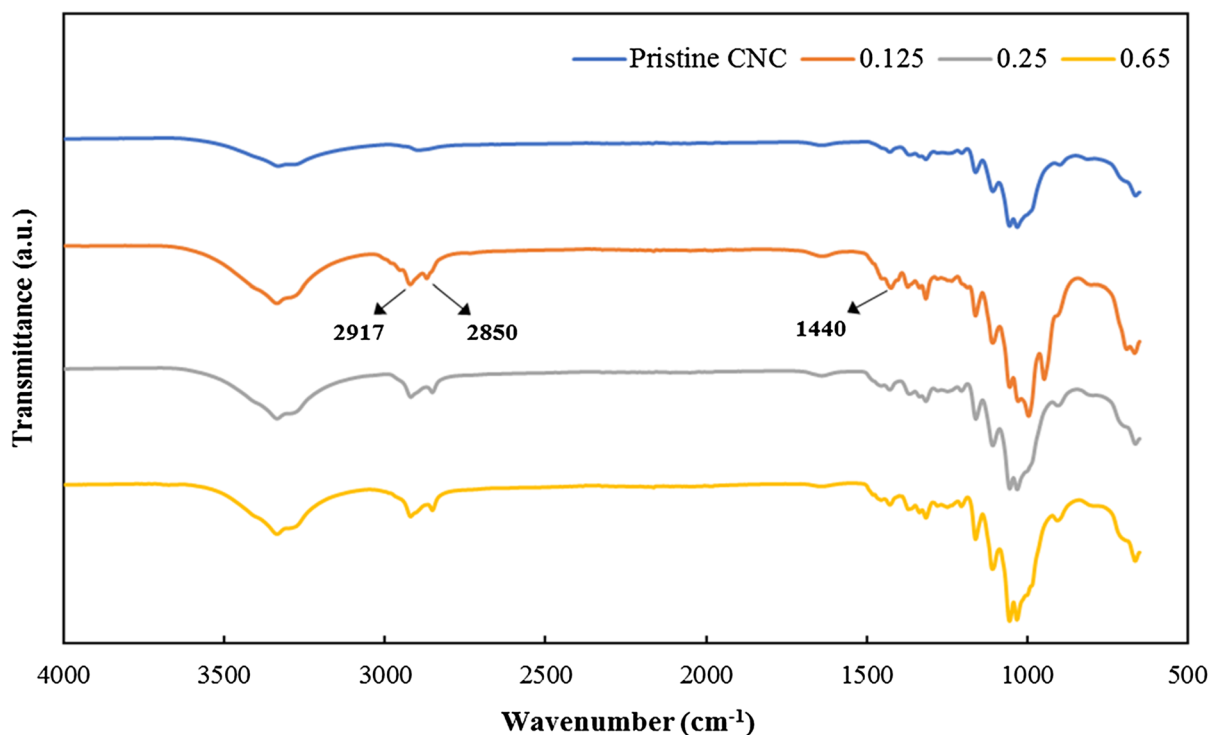


Fig. 1 FTIR spectra of pristine CNC, and MCNC 0.125, 0.25 and 0.65

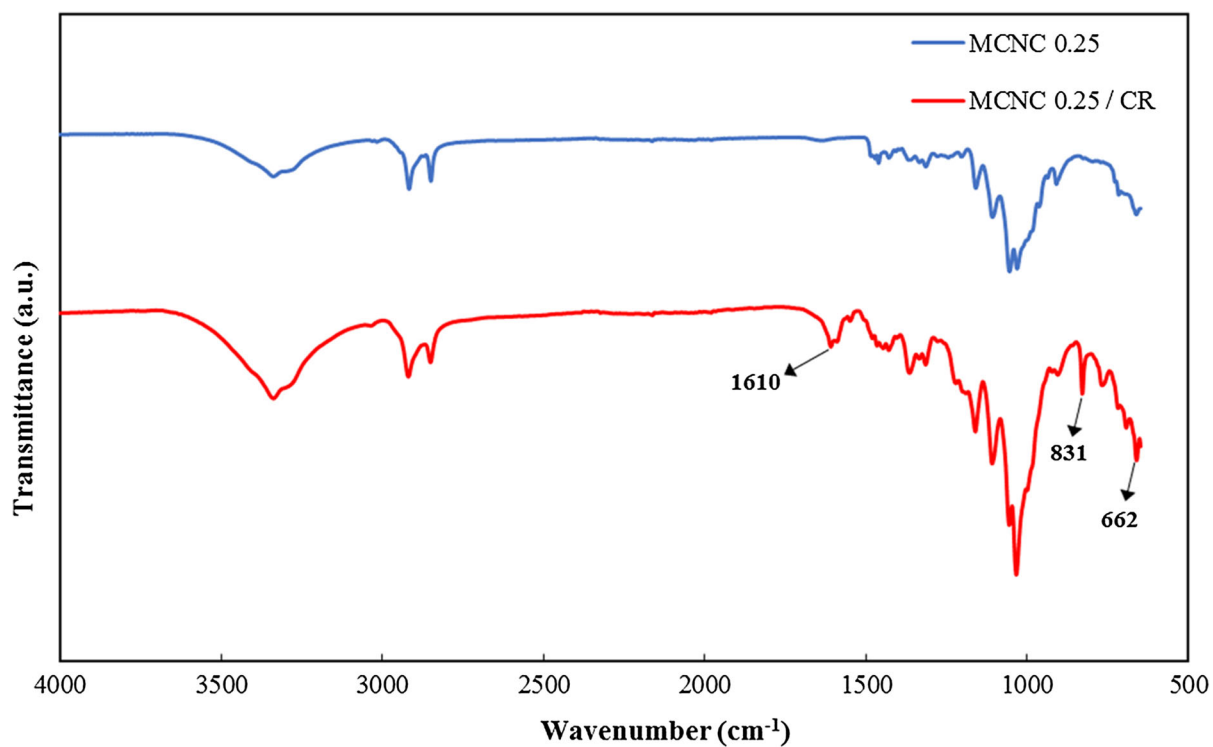


Fig. 2 FTIR spectra of MCNC 0.25 before and after CR adsorption

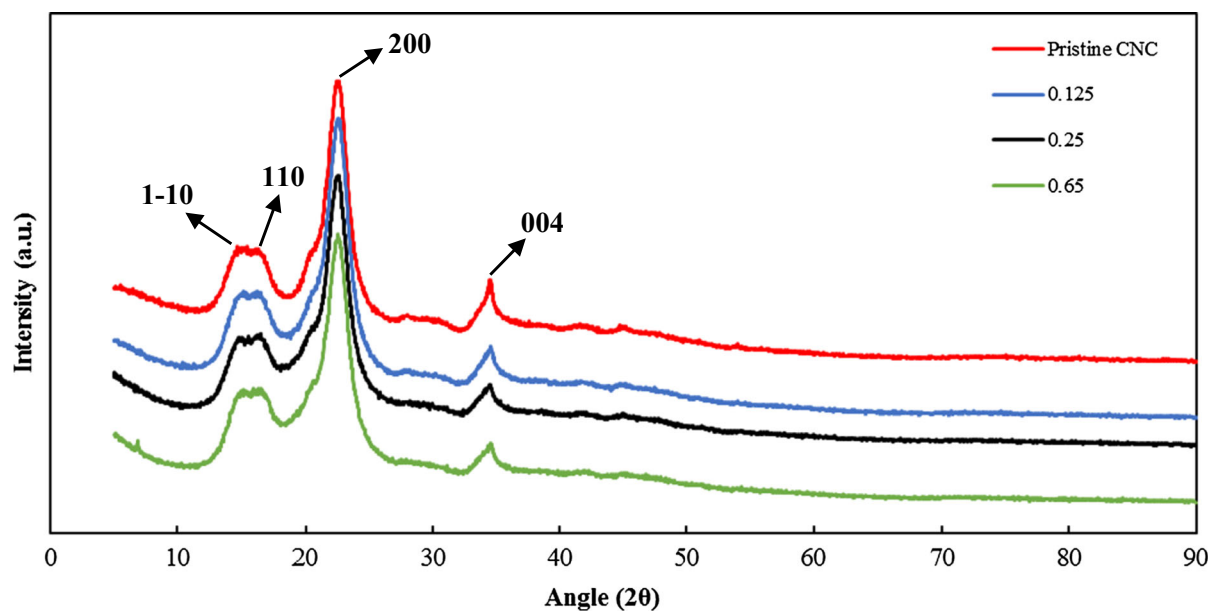


Fig. 3 XRD patterns of pristine CNC, MCNC 0.125, MCNC 0.25 and MCNC 0.65

XRD analysis

The peaks at 14° , 16° , 22.5° and 34.6° 2θ are present for all modified samples as seen in Fig. 3. These peaks correspond to the planes (1–10), (110), (200) and (004), respectively, of cellulose I in CNCs (French 2014; Ling et al. 2019). Based on the obtained results, this modification has not changed the crystalline structure of MCNC particles and adjustments have only taken place on their surface, although small changes in the crystalline structure could be better appreciated by Rietveld refinement (Meza-Contreras et al. 2018; Ling et al. 2019). Furthermore, it is concluded that all crystalline quaternary ammonium salts were successfully removed from the surface of CNC particles. The XRD patterns for the rest of the MCNC samples are included in the supplementary information (Fig. S2 and S3).

Effect of modification on the surface charge of CNC particles

The surface charge of adsorbents plays an important role in the adsorption of ionic dyes, such as CR, since electrostatic attraction is one of the dominant adsorption mechanisms. Previous studies suggest that addition of surfactants to CNC suspensions alter the surface charge of CNC particles, which could also affect the interactions between nanoparticles (Prathapan et al. 2016). Therefore, modification with surfactants would probably affect the adsorption properties of CNCs to a great extent. Preliminary experiments indicated that pristine CNC does not adsorb CR (at all examined agitation times and CR concentrations) presumably due to repulsion from the negative surface charge of CNC particles. Figure 4 shows the equilibrium adsorption capacities of CNCs modified with various amounts of CTAB. As the weight fraction of CTAB increased until 0.24 w/w, the adsorption capacity of CR onto MCNC increased, with the adsorption capacity leveling at 220 mg g^{-1} and remained relatively constant as the weight fraction of CTAB reached 1 w/w. This behavior is attributed to the changes in the overall surface charge density of CNC particles.

Zeta potential measurements were performed to investigate the extent of surface charge change of CNC particles. Figure 5 depicts the zeta potential of CNC and MCNC samples.

The pristine CNC suspension shows a zeta potential of -55 mV . Upon addition of CTAB to the CNC suspension, the cetyltrimethylammonium cations (CTA^+) are absorbed to the surface of the CNC particles with their cationic headgroup facing towards the particles, Fig. 6a. This absorption takes place due to the electrostatic attraction between the positively charged headgroup of cetyltrimethylammonium cations and negatively charged sulfate ester groups on the surface of CNC particles (Hu et al. 2015). As the concentration of CTAB increases, more surfactant molecules are adsorbed to the surface of CNC particles up to the point where the negative charges on the surface of CNCs are neutralized by the positive charges of the surfactant. At this point the zeta potential becomes zero. Further increase in the concentration of CTAB results in the formation of admicelles on the surface of CNC particles, as shown in Fig. 6b. This is attributed to the hydrophobic attraction between the hydrophobic tails of the bound and free surfactant molecules. Therefore, a surface charge reversal takes place, and the zeta potential becomes more positive as the surfactant concentration increases. Nevertheless, the surface of CNC particles saturates with surfactant molecules at a critical concentration after which further addition of CTAB results in the formation of free micelles as depicted in Fig. 6c. This critical concentration is slightly larger than the critical micelle concentration (CMC) of CTAB, namely 1 mM (Prathapan et al. 2016). In addition, this slight difference is attributed to the presence of CNCs in the medium postponing the formation of free micelles due to the adsorption of surfactant molecules (Penfold et al. 2007; Dhar et al. 2012). Hence, surfactant addition does not change the net surface charge of CNC particles above the critical concentration. In previous studies, a similar trend was observed for the change in the zeta potential of cellulosic surfaces, including films (Penfold et al. 2007), fibers (Alila et al. 2005) and nanocrystals (Salajková et al. 2012), as a result of their interaction with quaternary ammonium surfactants.

The equilibrium adsorption capacity and zeta potential values exhibit a slight drop after CTAB weight fraction of 0.25 w/w, which seems to be within experimental error in the case of adsorption capacities. Nevertheless, this observation could be attributed to the fact that further addition of surfactant above 0.25 w/w would result in an increase of the overall ionic

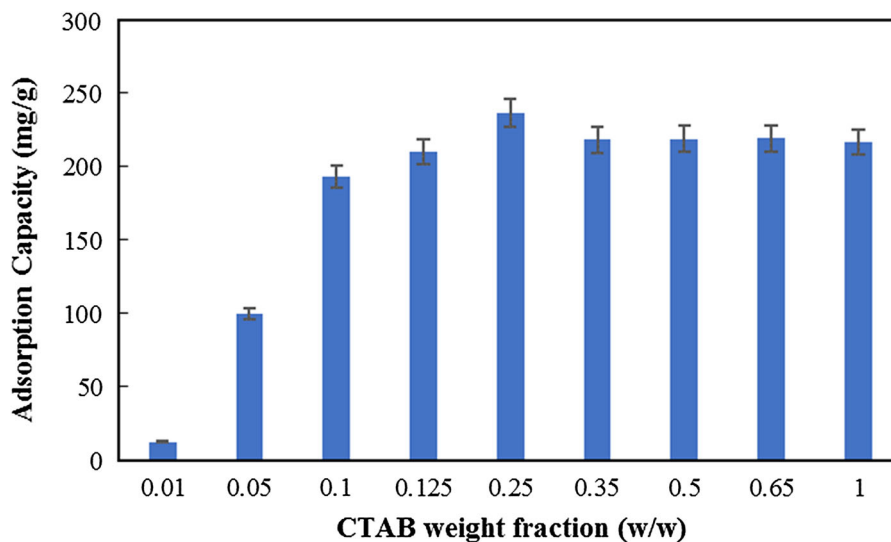


Fig. 4 Effect of CTAB weight fraction (w/w) on the adsorption capacity of MCNCs. Experimental conditions: dye concentration, 100 mg L^{-1} ; dosage, 10 mg/50 mL ; pH, 7.5; temperature, $25 \text{ }^\circ\text{C}$; equilibration time, 90 min

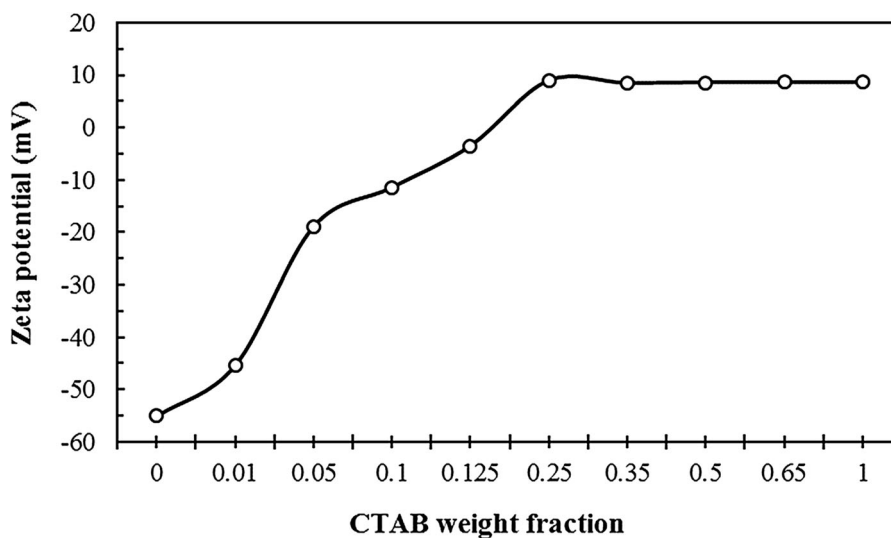


Fig. 5 Effect of CTAB weight fraction on zeta potential of CNC and modified CNC samples. The zeta potential is proportional to the surface charge of the particles

strength as well as a rearrangement of the CNC bound surfactant molecules, admicelles, and free micelles (Hu et al. 2015). Depending on the extent of the modification, the dominant adsorption mechanism might be different for different modified samples. The adsorption mechanisms are discussed in detail below.

Adsorption kinetics

The adsorption kinetics of modified CNCs were investigated in order to gain a better understanding of the mechanism of adsorption. The effect of time on the adsorption of CR is shown in Fig. 7. The adsorption capacity rose above 100 mg g^{-1} in only 5 min. This rapid increase in the adsorption of CR is attributed to the abundance of active adsorption sites

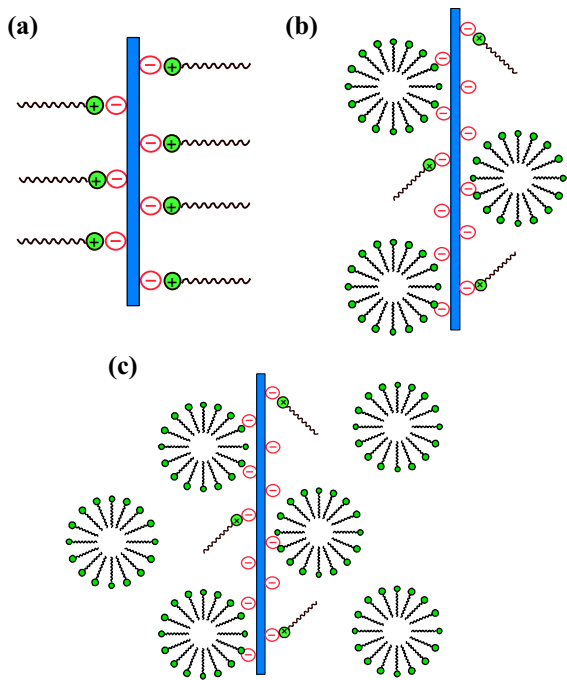


Fig. 6 Schematic illustration of CTAB/CNC interactions

in the beginning, and the significant adsorption driving force resulting from the large difference between the concentration of dye molecules in the solution and the surface of the MCNC particles. The increase of the adsorption capacity continues with a modest slope for roughly 80 min and reaches a plateau that lasts up to about 90 min. This implies that over a short period after the beginning of the adsorption process, the remaining vacant sites become sterically hindered by

the already bound dye molecules (Zhou et al. 2013). Therefore, the adsorption proceeds with a lower rate until it reaches equilibrium. It was observed that the adsorption capacity reaches its maximum, namely q_e , after 90 min, about the same for all samples. Although the adsorption of CR onto MCNC was monitored up to 200 min, the adsorbent starts desorbing the dye molecules after about 90 min and remains constant afterwards. Hence, we conclude that the adsorption equilibrium time for MCNC is about 90 min.

The adsorption kinetics were further analyzed by examining three kinetic models: a pseudo-first order, a pseudo-second order, and intraparticle diffusion model.

The pseudo-first order and pseudo-second order are two of the most commonly used models for investigating the mechanism of adsorption and determining the adsorption rate constants. The linear forms of these equations are expressed as:

$$\ln(q_e - q_t) = \ln(q_e) - K_1 t \quad (4)$$

$$\frac{t}{q_t} = \frac{1}{k_2 q_e^2} + \frac{t}{q_e} \quad (5)$$

where q_e is the equilibrium adsorption capacity of modified CNCs, and K_1 (min^{-1}) and K_2 ($\text{g mg}^{-1} \text{min}^{-1}$) are the rate constants of pseudo-first order and pseudo-second order models, respectively. The experimental data were fitted using Eqs. (4) and (5). The results are shown in Fig. 8, and the equilibrium parameters and correlation coefficients (R^2) are summarized in Table 1. For all

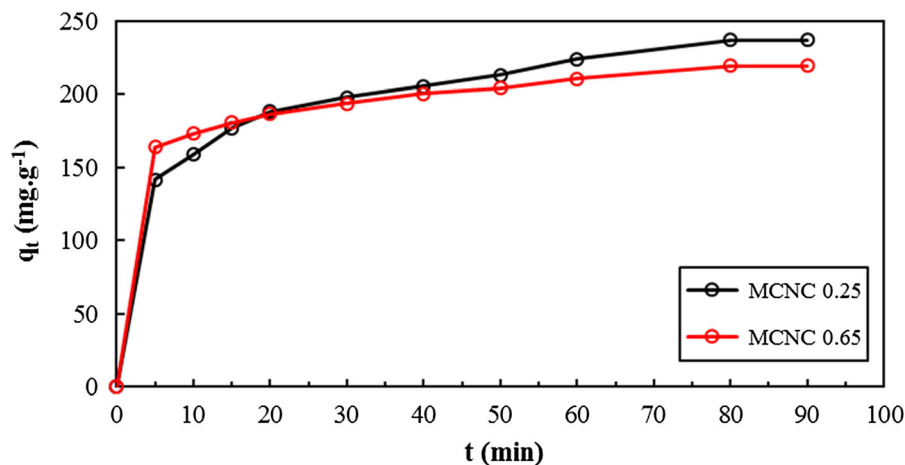


Fig. 7 The effect of contact time on the dye adsorption of MCNC 0.25, and 0.65

modified CNC samples, the value of R^2 is almost equal to unity for the pseudo-second order model. Furthermore, the theoretical q_e calculated using the pseudo-second order model agrees with the equilibrium capacities obtained from the experimental results listed in Table 1. Comparing these parameters with the ones obtained from the pseudo-first order model implies that the adsorption of Congo red dye by the modified CNCs can be well described by the pseudo-second order model.

The intra-particle diffusion model was used to further investigate the adsorption mechanism of CR by modified CNC and examine any possible rate-controlling steps. The intra-particle diffusion model is expressed as:

$$q_t = K_i t^{1/2} + C \quad (6)$$

where K_i ($\text{mg g}^{-1} \text{min}^{-0.5}$) is the rate constant of intra-particle diffusion model, and C is a constant representing the extent of the boundary layer effect. As shown in Fig. 9, the plot of q_t versus $t^{1/2}$ exhibits a change in slope implying that surface adsorption is not the only mechanism controlling the adsorption process. In fact, the adsorption process consists of two steps. First, the dye molecules are transported from the bulk solution to the external surface of the adsorbent by boundary layer diffusion. Second, the dye molecules diffuse from the external surface into the porous structure of the adsorbent (Tang et al. 2012).

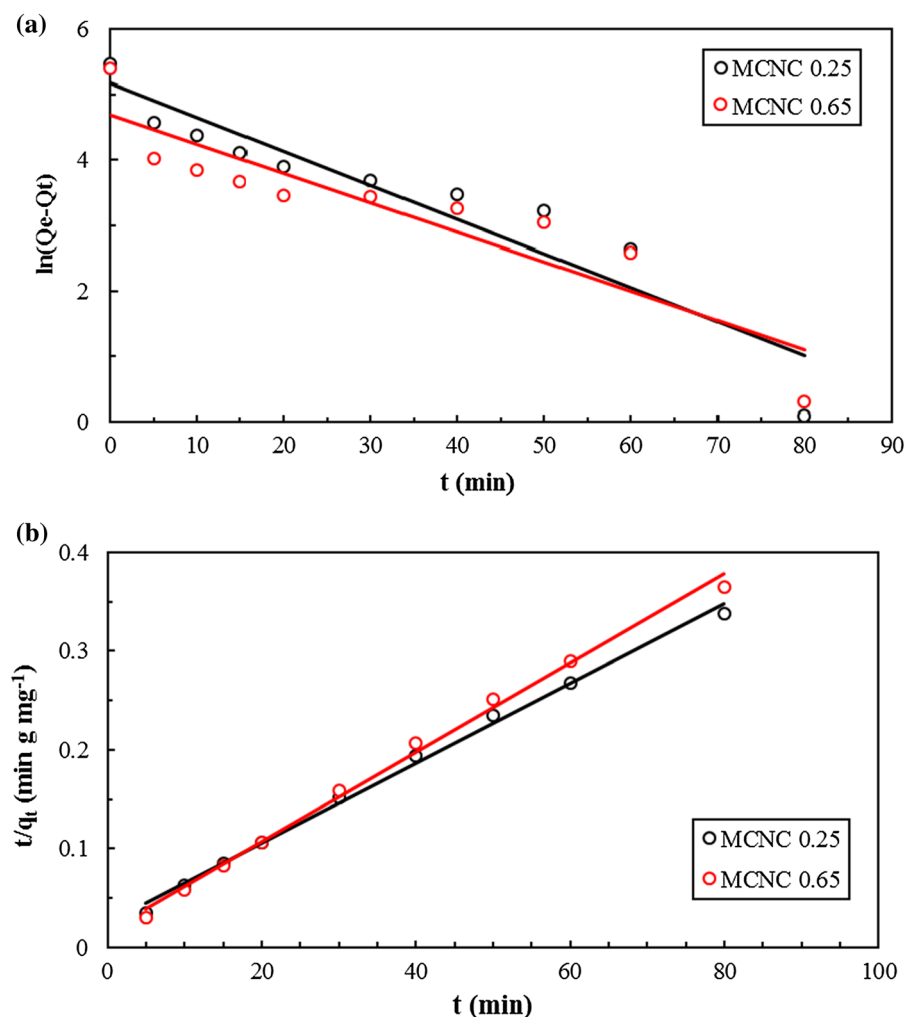
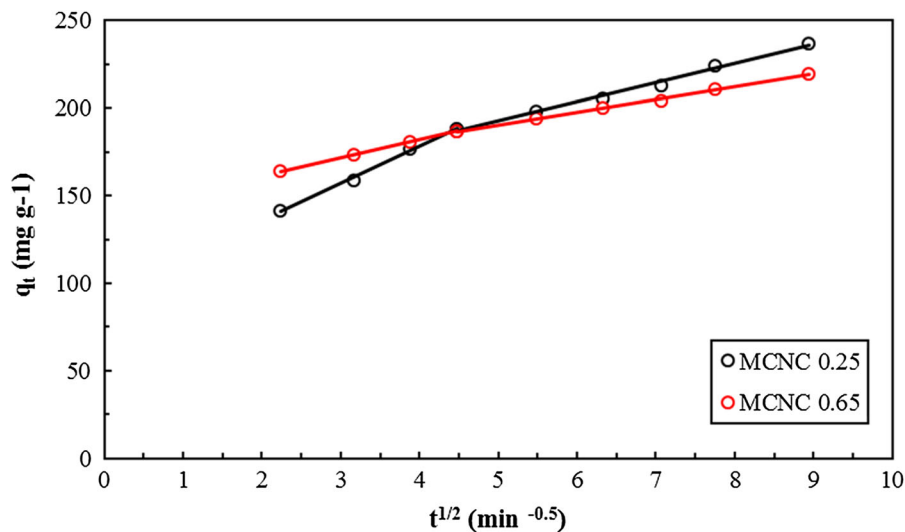


Fig. 8 Linear regression of adsorption kinetic models for MCNC 0.25, and 0.65. A pseudo-first order, b pseudo-second order. Experimental conditions: dye concentration, 100 mg L^{-1} ; dosage, $10 \text{ mg}/50 \text{ mL}$; pH, 7.5; temperature, $25 \text{ }^\circ\text{C}$

Table 1 Adsorption kinetic parameters of CR onto MCNC 0.25, and MCNC 0.65

Sample	Experiment $q_{e,exp}$ (mg g ⁻¹)	Pseudo-first order kinetic model			Pseudo-second order kinetic model		
		$q_{e,cal}$ (mg g ⁻¹)	K_1 (h ⁻¹)	R^2	$q_{e,cal}$ (mg g ⁻¹)	K_2 (g mg ⁻¹ h ⁻¹)	R^2
MCNC 0.25	244	179	0.119	0.870	246	0.00065	0.994
MCNC 0.65	219	120	0.115	0.804	217	0.00173	0.995

**Fig. 9** Intra-particle diffusion model of CR adsorption onto MCNC 0.25, and 0.65. Experimental conditions: dye concentration, 100 mg L⁻¹; dosage, 10 mg/50 mL; pH, 7.5; temperature, 25 °C

The equilibrium parameters for the intra-particle diffusion model are listed in Table 2. None of the C values are zero at either stage, indicating that intra-particle diffusion is not the sole dominant adsorption mechanism. Intra-particle diffusion plays an important role in the adsorption process. At the first stage, the value of the intra-particle diffusion rate constant, K_i , is the highest for MCNC 0.25, which is most likely attributed to its larger surface charge density and more active adsorption sites compared to the other samples.

Adsorption isotherms

Adsorption isotherms were examined over the CR concentration range of 50–400 mg L⁻¹ to further investigate the mechanism of adsorption and evaluate the adsorption properties of modified CNCs. In this study, two classic isotherm models, Langmuir and Freundlich, were used to determine the equilibrium isotherm parameters of the adsorbent.

The Langmuir isotherm describes a monolayer adsorption process with homogenous distribution of

Table 2 Intra-particle diffusion parameters for adsorption of CR onto MCNC 0.25, and MCNC 0.65

Sample	First stage			Second stage		
	C_1 (mg g ⁻¹)	K_1 (mg g ⁻¹ min ^{-0.5})	R_1^2	C_2 (mg g ⁻¹)	K_2 (mg g ⁻¹ min ^{-0.5})	R_2^2
MCNC 0.25	93.33	21.28	0.995	137.86	10.96	0.992
MCNC 0.65	139.48	10.78	0.998	154.18	7.24	0.997

the adsorption sites on the surface of the adsorbent (Kumar and Sivanesan 2005). The linear form of the Langmuir model is expressed as:

$$\frac{C_e}{q_e} = \frac{C_e}{q_m} + \frac{1}{q_m K_L} \quad (7)$$

where C_e (mg L^{-1}) is the equilibrium concentration of the dye solution, q_e (mg g^{-1}) is the adsorption capacity at equilibrium, and q_m (mg g^{-1}) is the maximum amount of CR adsorbed per unit mass of adsorbent.

The Freundlich isotherm is an empirical model assuming that the adsorption process is a multilayer process and takes place on heterogeneous surfaces (Foo and Hameed 2010). The linear form of this model is:

$$\ln(q_e) = \ln K_F + \frac{1}{n} \ln C_e \quad (8)$$

where K_F (L mg^{-1}) is a Freundlich constant related to the adsorption capacity, and $1/n$ corresponds to the heterogeneity of the adsorption surface, indicating the favorability of the adsorption process.

The isotherm study was conducted on the optimum sample, MCNC 0.25, at three temperatures to investigate the temperature effect on the maximum adsorption capacity. Experimental data were fitted to both isotherm models, and the results are presented in Fig. 10. The isotherm parameters and correlation coefficients (R^2) are summarized in Table 3. Based on the obtained results, the values of R^2 are larger than 0.994 at all temperatures indicating that the Langmuir model provides a better description of the adsorption isotherm. Furthermore, the theoretical q_m values calculated from Langmuir model are in good agreement with the experimentally obtained q_m values. This implies that the adsorption of CR onto MCNC is mostly monolayer, and the adsorption sites on the surface of the adsorbent are identical. In addition, the q_m and K_L values decrease with temperature indicating the exothermic nature of the adsorption process.

According to Freundlich model, the value of the heterogeneity constant ($1/n$) was calculated to examine the favorability of the interaction between dye molecules and adsorbent. Based on the results listed in Table 3, the values of ($1/n$) are in the range of 0–1 and increase with temperature, implying that the adsorption process is favorable at all temperatures, and the increase of temperature is not in favor of the adsorption process. In addition, the values of the Freundlich

constant, K_F , decrease with temperature, which further supports the exothermic nature of the adsorption process.

Table 4 shows the value of maximum experimental adsorption capacity ($q_{m,exp}$) of Congo red on several cellulose based adsorbents synthesized in the recent years. Based on Table 4, the maximum adsorption capacities are in the range of 40–600 mg g^{-1} which implies that MCNC is a suitable and comparable adsorbent for the adsorption of CR in aqueous medium.

Thermodynamic study

To study the effect of temperature on the adsorption of CR by modified CNC, the thermodynamics of the system were analyzed at three temperatures, 25, 35 and 45 °C over the concentrations 100–400 mg L^{-1} . The change in enthalpy (ΔH^0), entropy (ΔS^0) and Gibbs free energy (ΔG^0) were determined using the following equations (Zhu et al. 2011):

$$\Delta G^0 = -RT \ln K_C \quad (9)$$

$$\ln K_C = -\frac{\Delta H^0}{RT} + \frac{\Delta S^0}{R} \quad (10)$$

where R ($8.314 \text{ J mol}^{-1} \text{ K}^{-1}$) is the ideal gas constant, T (K) is the absolute temperature and K_C is the Langmuir constant. Based on Eq. (10), ΔH^0 and ΔS^0 are calculated using the slope and intercept of the linear plot $\ln K_C$ versus $1/T$.

The values of the thermodynamic parameters and Langmuir constant at each temperature are summarized in Table 5. Based on the results in Table 5, the negative values of Gibbs free energy at three experimental temperatures imply that the adsorption of CR onto modified CNC is spontaneous. Furthermore, as the temperature increased from 298 to 318 K, the absolute values of Gibbs free energy decreased meaning that adsorption process is more favorable at lower temperatures. Generally, the value of Gibbs free energy between 0 and -20 kJ mol^{-1} indicates that the adsorption mechanism is physisorption, while the value in between -80 and -400 kJ mol^{-1} indicates a chemisorption process (Wu et al. 2013). Based on the values of ΔG^0 in Table 5, the adsorption of CR by modified CNC involves both chemisorption and physisorption. The values of ΔH^0 and ΔS^0 are found

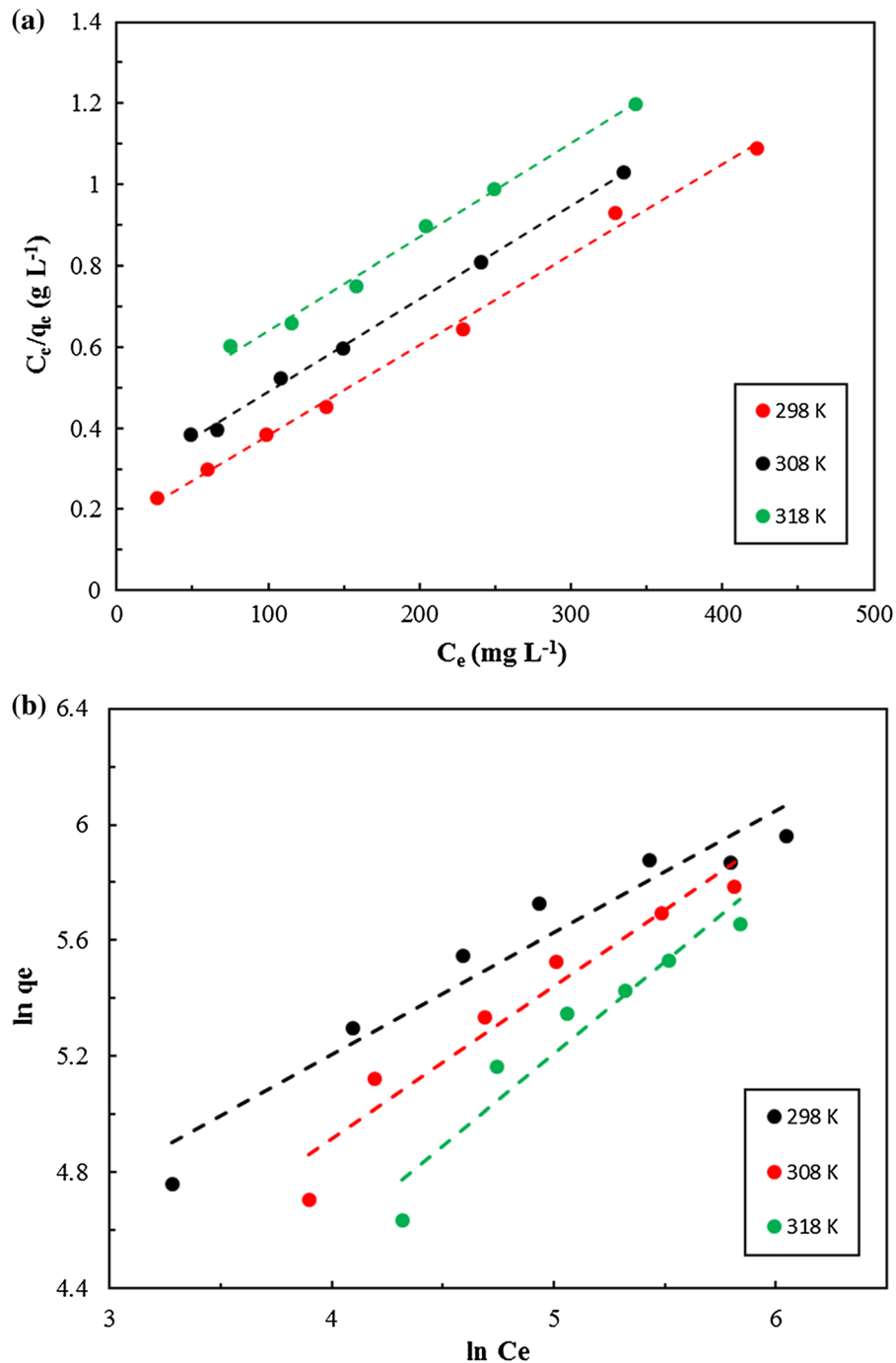


Fig. 10 Linear regression of isotherm models for adsorption of CR onto MCNC 0.25 at 298, 308, and 318 K. **a** Langmuir model, **b** Freundlich model. Experimental conditions: dosage, 10 mg/50 mL; pH, 7.5

from the plot of $\ln K_C$ versus $1/T$ to be equal to $-35.45 \text{ kJ mol}^{-1}$ and $0.018 \text{ J mol}^{-1} \text{ K}^{-1}$, respectively. The negative value of ΔH^0 reveals the exothermic nature of the adsorption process.

Adsorption mechanism

Electrostatic attraction is one of the most effective factors in adsorption. Based on the values of zeta

Table 3 Isotherm parameters of Langmuir and Freundlich model for the adsorption of CR onto MCNC 0.25

T (K)	Langmuir model			Freundlich model		
	q_m (mg g ⁻¹)	K_L (L mg ⁻¹)	R^2	K_F (L mg ⁻¹)	$1/n$	R^2
298	448.43	13.89	0.996	34.04	0.42	0.933
308	436.68	8.80	0.998	16.64	0.53	0.935
318	432.90	5.65	0.994	7.61	0.64	0.923

Table 4 Maximum adsorption capacity for CR on various cellulose based adsorbents

Adsorbent	q_m (mg g ⁻¹)	References
CTAB modified CNC	448	Present work
Imidazolium ionic liquid modified cellulose	563	(Zhang et al. 2018)
Magnetic nanocellulose based ionic liquid	131	(Beyki et al. 2016)
Crosslinked cellulose dialdehyde	42	(Kumari et al. 2016)
Cellulose/chitosan composite	382	(Wang et al. 2018b)
CTAB impregnated chitosan hydrogel	272	(Chatterjee et al. 2011)
Poly(<i>N,N</i> -dimethylacrylamide- <i>co</i> -acrylamide) grafted hydroxyethyl cellulose hydrogel	102	(Jana et al. 2018)

Table 5 Thermodynamic parameters of CR adsorption onto MCNC 0.25

$T(k)$	Q_m (mg g ⁻¹)	K_L (L mg ⁻¹)	ΔG^0 (kJ mol ⁻¹)	ΔH^0 (kJ mol ⁻¹)	ΔS^0 (J mol ⁻¹ K ⁻¹)
298	448.43	13.89	- 23.66	- 35.45	0.018
308	436.68	8.80	- 23.27		
318	432.90	5.65	- 22.85		

potential for the modified CNC samples (Fig. 5) and the S/N ratios (Table S1), at CTAB weight fractions larger than 0.25 w/w, the CTA⁺ cations predominantly exceed the sulfate groups (SO₃⁻) on the surface of modified CNCs, and their overall surface charge becomes positive, indicating that electrostatic attraction between the negative charges of CR and positive sites of MCNC is responsible for the adsorption of CR. However, at weight fractions lower than 0.125 w/w, the overall charge density on the surface of MCNC is negative indicating that CR molecules should be repelled, and adsorption of CR should not have happened. Nevertheless, the nonzero adsorption capacity of MCNC even at 0.01 w/w of CTAB suggests that electrostatic attraction is not the sole mechanism of adsorption, and other mechanisms are also involved in the adsorption process. Furthermore,

the amount of CTAB used in the modification step might affect the existence or dominance of each mechanism.

To explore the existence of various adsorption mechanisms, FTIR spectra of CR and the optimum sample, MCNC 0.25, were investigated before and after adsorption (Fig. 11). Based on Fig. 11, the absorption peak at 3340 cm⁻¹, corresponding to the -OH stretching vibration of MCNC, slightly shifted, intensified and expanded after adsorption. The absorption peaks at 3468 cm⁻¹, corresponding to the -NH₂ groups of CR, and 1583 cm⁻¹, corresponding to -N=N- stretching of CR, diminish after adsorption. This verifies that hydrogen bonding between -NH₂ and -N=N- groups of CR and hydroxyl groups of MCNC is one of the major mechanisms involved in the adsorption of CR onto MCNC (Liu et al. 2014; Wu

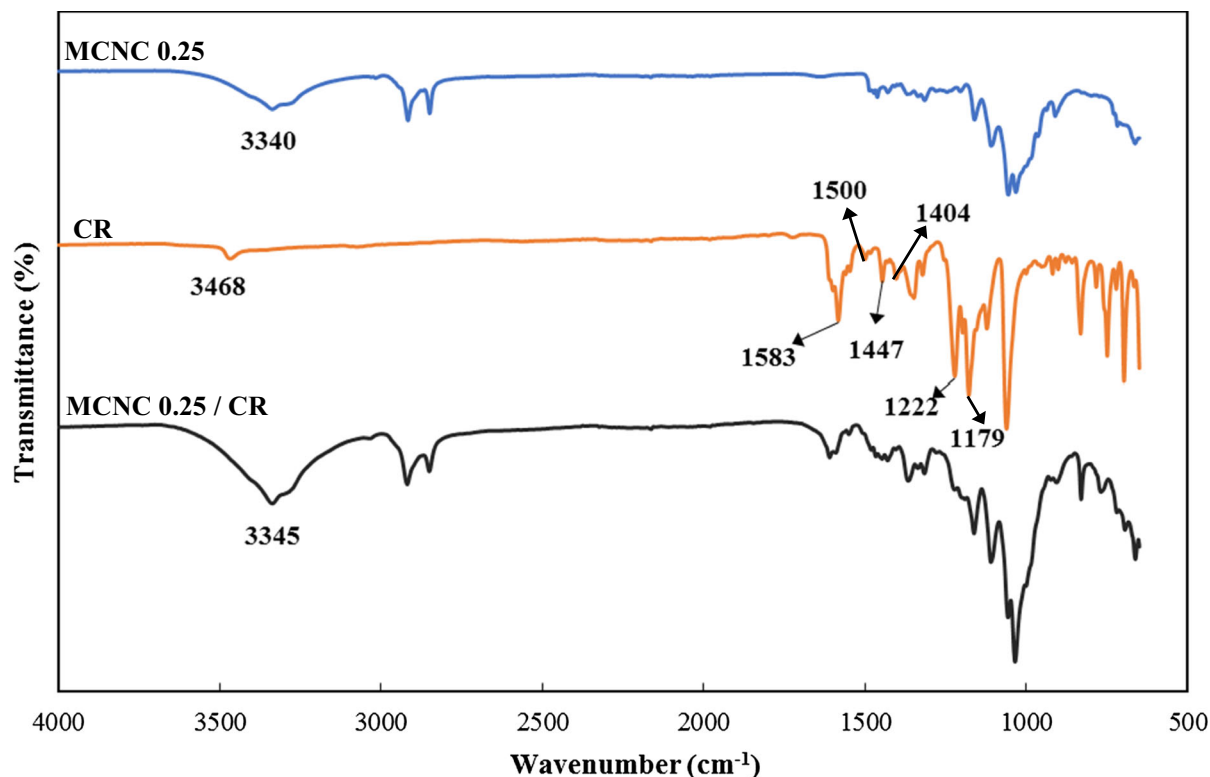


Fig. 11 FTIR spectrum of CR and MCNC 0.25, before and after CR adsorption

et al. 2014). In addition, two adsorption peaks at 1179 and 1222 cm^{-1} , corresponding to the sulfonate groups (SO_3^-) of CR, slightly shift and diminish considerably after adsorption. This implies that sulfonate groups of CR are involved in the adsorption process and could be attracted to MCNC through both hydrogen bonding, with hydroxyl groups, and electrostatic attraction with the positive heads of the bound micelles, namely N^+ (Wang and Wang 2008).

Hydrophobic attraction between hydrophobic parts of CR and alkyl tail of single CTA^+ molecules bound to the surface of CNCs is believed to be another mechanism engaged in the adsorption of CR onto MCNC which is further approved by the FTIR spectra (Fig. 11) where the absorption peaks at 1500, 1447 and 1404 cm^{-1} , corresponding to the aromatic rings in the structure of CR, have been widened, shifted and reduced implying their involvement in the adsorption process (Liu et al. 2014; Beyki et al. 2016). This would be the case especially at low weight fractions of CTAB where the S/N ratio (Table S1) is larger than 1 implying the dominance of negative sulfate ester groups (SO_3^-) in the structure of adsorbent. This is

further supported by the zeta potential values (Fig. 5) as the MCNCs exhibit an overall negative surface charge at CTAB weight fractions lower than 0.125. This could suggest that despite the existence of bound micelles (with positive N^+ heads) on the surface of CNCs, the single CTA^+ molecules (Fig. 6a) are involved in the adsorption of CR onto the surface of MCNC. Hence, hydrophobic attraction plays a more important role in the adsorption process compared to electrostatic interactions for samples with negative zeta potential. Similar to the samples with positive zeta potential, hydrogen bonding is another mechanism responsible for the adsorption of CR onto MCNC when the overall charge density on the surface of adsorbent particles is negative.

The morphology of the adsorbent is another factor that influences the adsorption process. The intraparticle diffusion kinetic model suggested that the morphology of MCNC might play an important role in the adsorption process. To examine the morphology of MCNC and its potential effect on the adsorption of CR, scanning electron micrograph (SEM) images of

MCNCs were taken at different weight fractions of CTAB, Fig. 12.

The SEM images reveal that addition of CTAB have resulted in the aggregation of CNCs in the form of fluffy bundles even at the lowest weight fraction of CTAB (MCNC 0.01), Fig. 12a. As the concentration of CTAB increases, the CNC aggregates form a layered structure with bigger particles, as depicted in Fig. 12b, c. Finally, at the optimum weight fraction of CTAB (MCNC 0.25), the CNC aggregates have formed a porous structure, Fig. 12d, which could be responsible for the intra-particle diffusion of dye molecules into the adsorbent particles. Furthermore, based on the scales shown on the SEM micrographs, the increase in the size of the MCNC particles with addition of surfactant could be inferred.

As previously discussed, the addition of CTAB to CNC suspensions results in the formation of admicelles on the surface of the particles above a critical

concentration. The electrostatic attraction between the positive heads of the admicelles on one CNC particle with the negative parts of its neighboring particles would result in the formation of CNC bundles as depicted in Fig. 13. The aggregation of CNCs, referred to as polymer induced micellization (Dhar et al. 2012), generates pores between the particles that set the stage for the intra-particle diffusion of dye molecules into the adsorbent. Figure 14 shows the schematic of the mechanisms during the adsorption of CR onto MCNC.

Adsorbent stability in aqueous media

MCNCs were washed several times to remove unbound surfactant molecules on the surface of the CNC particles, and thus the adsorbent does not introduce any surfactant molecules into the solution. The number of cycles required to wash all the unbound

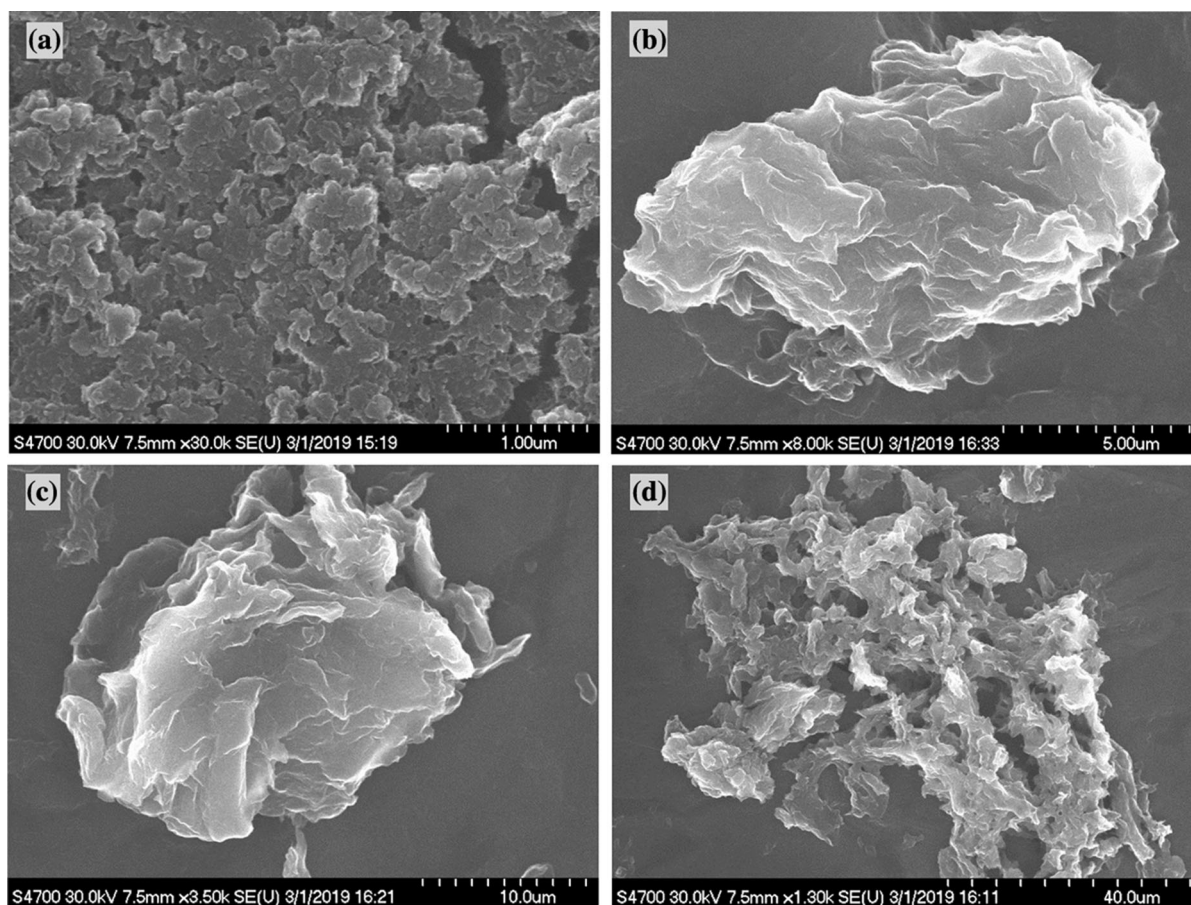


Fig. 12 SEM micrographs of MCNC **a** 0.01, **b** 0.05, **c** 0.125, **d** 0.25

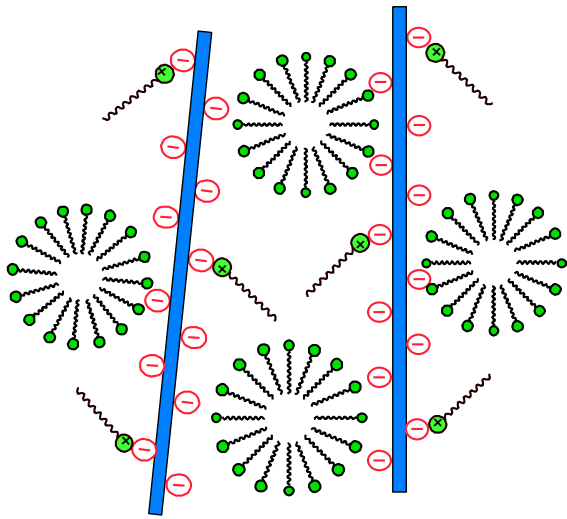


Fig. 13 Polymer induced micellization of CNC rods

surfactant molecules from the surface of MCNC depends on the amount of surfactant used for the modification. The XRD patterns of MCNC did not show any peaks from crystalline CTAB, suggesting unbound surfactant was absent. Table 6 shows the number of washing cycles required for different MCNC samples.

MCNC 0.35 and MCNC 0.65 were chosen for further investigation on the effect of successive cycles of washing on the adsorption capacity of adsorbent. Figure 15 shows the change in the equilibrium adsorption capacity of MCNC 0.35 and MCNC 0.65 with the number of washing cycles. The samples contain a large amount of CTAB crystals right after the synthesis as indicated by XRD, Figs. S3b and S3c. Therefore, other than the adsorption of CR by modified CNC particles, the surfactant and CR

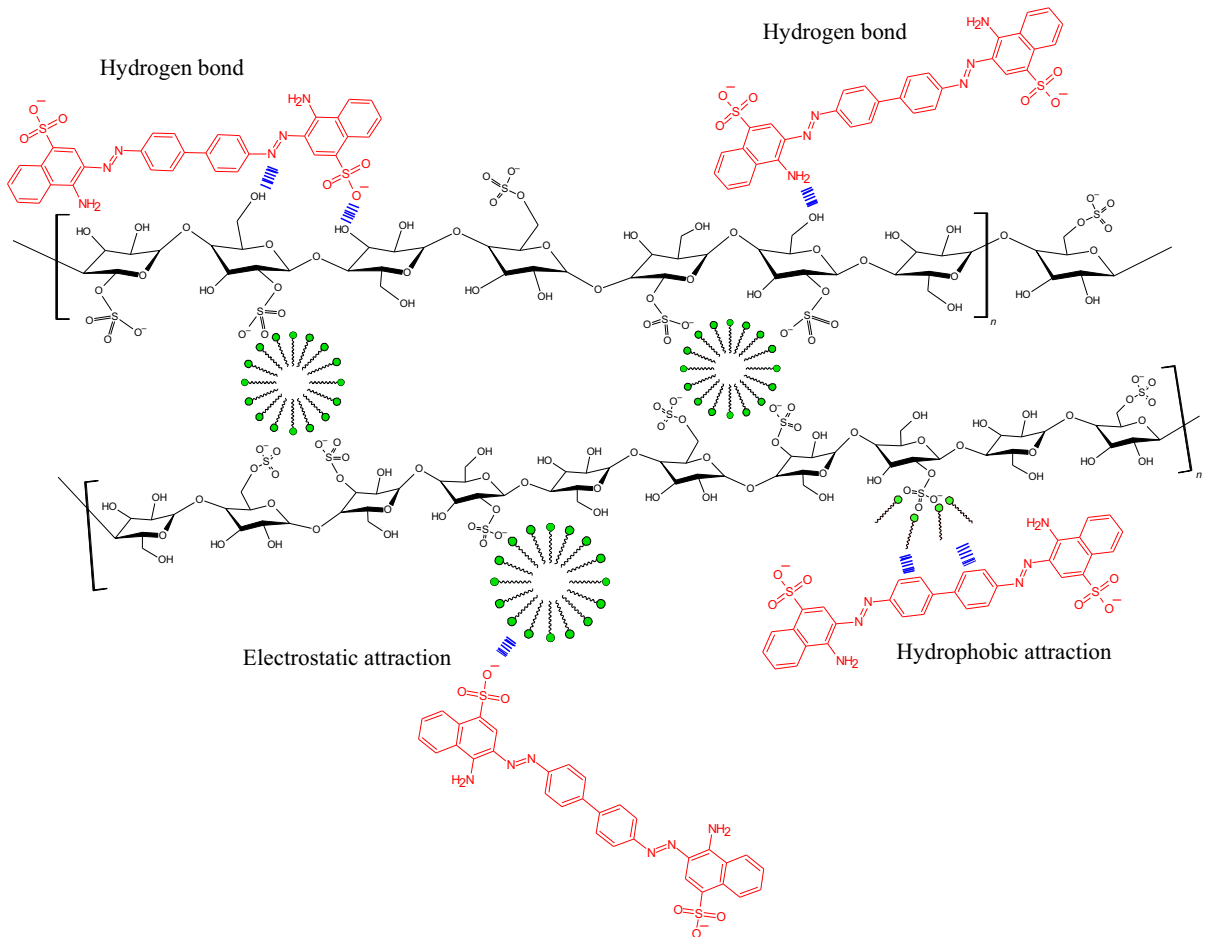


Fig. 14 Schematic of various active adsorption interactions during the adsorption of CR onto MCNC

Table 6 Number of required washing cycles during synthesis process

Sample ID	MCNC 0.01	MCNC 0.05	MCNC 0.1	MCNC 0.125	MCNC 0.25	MCNC 0.35	MCNC 0.65	MCNC 1
# Required washing cycles	1	2	3	3	4	4	6	7

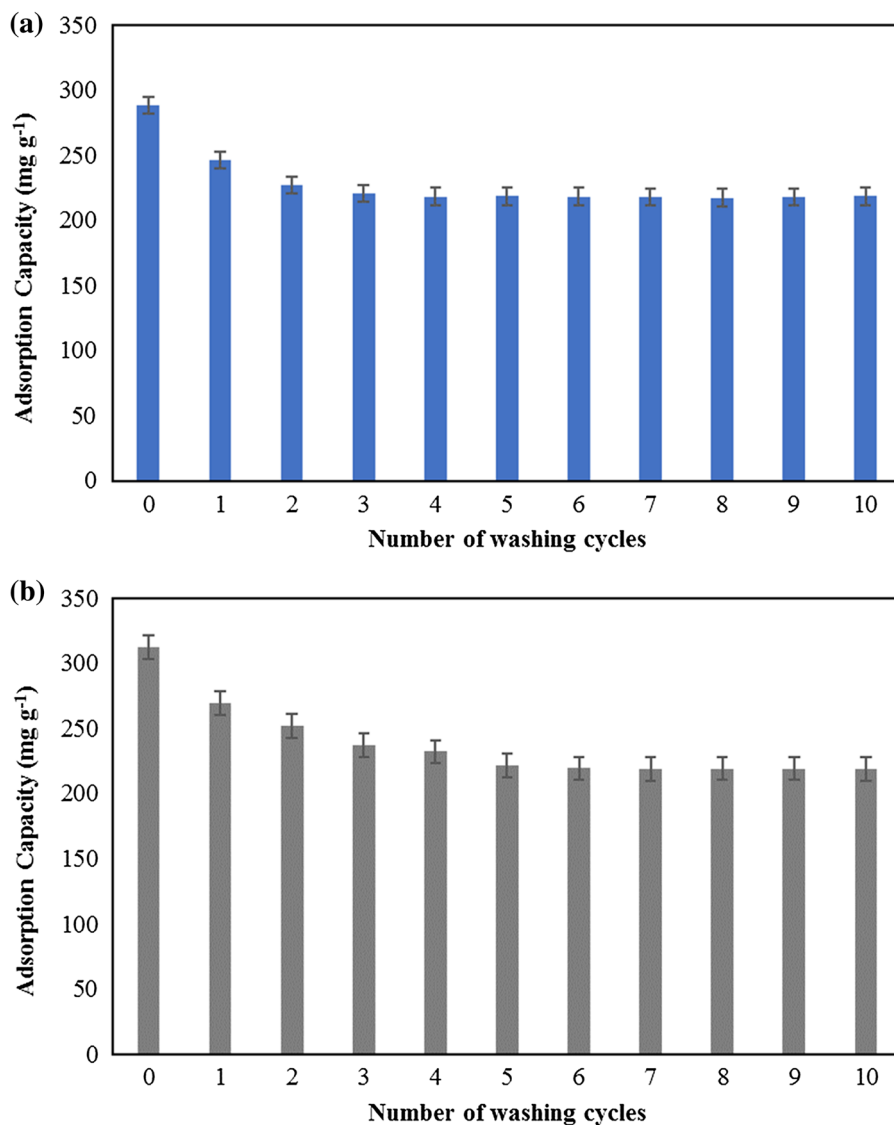


Fig. 15 Effect of successive washing cycles on the equilibration adsorption capacity of a MCNC 0.35 and b MCNC 0.65. Experimental conditions: dye concentration, 100 mg L⁻¹; dosage, 10 mg/50 mL; natural pH, 7.5; temperature, 25 °C; equilibrium time, 90 min

molecules are attracted to each other by electrostatic forces resulting in the precipitation of CR-CTAB complex. Before starting the washing cycles, MCNC

0.35 and 0.65 exhibit an equilibrium capacity of 288.44 and 312.36 mg g⁻¹ respectively. While washing cycles proceed, free surfactant molecules are

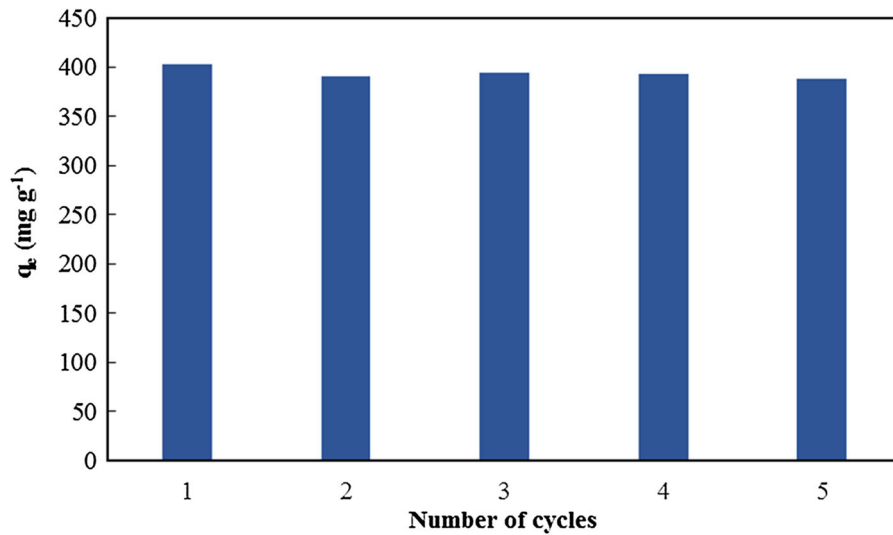


Fig. 16 Reusability of MCNC 0.25 for CR adsorption

removed gradually from the synthesized MCNC indicating that the apparent adsorption capacity would reduce. This downward trend in the adsorption capacities continue until the sample reaches the maximum number of required washing cycles. After this point, the adsorbent does not show any considerable changes in the adsorption capacity, and q_e remains roughly constant despite extra successive washing cycles. These results confirm the stability of MCNC in aqueous environment and against successive dialysis cycles.

Regeneration and reusability of a dye adsorbent is an important factor in evaluating its commercial applicability. To study the recyclability of MCNC, 5 cycles of adsorption/desorption were carried out on the optimum sample, MCNC 0.25, using ethanol, and the adsorption capacity was measured at the end of each cycle. Based on the results shown in Fig. 16, it can be seen that MCNC recovered over 85% of its original capacity after 5 cycles implying its good desorption ability.

Zeta potential measurement was performed on the adsorbent after each adsorption/desorption cycle and the results are shown in Fig. S4. Based on Fig. S4, the zeta potential values have slightly dropped after the first cycle and have remained roughly constant at subsequent cycles. This indicates that CTA⁺ cations, attached to the surface of MCNCs, are reasonably stable as the adsorbent exhibits positive values of zeta

potential with minor decrease over five adsorption/desorption cycles.

Furthermore, the adsorbent was thoroughly washed and freeze dried after the fifth cycle followed by grinding and sieving which yielded a powder. Besides, FTIR and SEM imaging was performed on the obtained powder and the results are shown in Fig. S5. Based on Fig. S5, MCNC has maintained its porous structure and exhibited similar peaks as its fresh adsorbent counterpart, although the intensity of signature peaks has been affected in some cases. Hence, the regeneration study indicated that MCNC is an effective adsorbent for the removal of anionic dyes.

Conclusions

Surfactant-modified CNC-based adsorbent was synthesized and used to examine its effectiveness for the adsorption of an anionic dye, Congo red. The characterization of adsorbent proved surface modification of CNCs, where the surfactant molecules had been absorbed through electrostatic attraction between the surfactant head group and negatively-charged sulfate half-esters of CNCs. As the weight fraction of surfactant increased, the number of micelles and single CTA⁺ molecules bound to the surface of CNCs increased. This resulted in a reduction in the negative charge density of CNC particles up to a point where

the charge density became positive. The samples exhibited an optimum at which the zeta potential and equilibrium adsorption capacity exhibited their maximum values. The experimental data were described well with both a pseudo-second order and intra-particle diffusion model indicating the existence of film-diffusion and intra-particle diffusion. This hypothesis was further supported by investigating the microstructure of MCNC showing its porous morphology. Isothermal studies at 298, 308, and 318 K on the optimum adsorbent concentration showed that the adsorption of CR onto MCNC is exothermic and spontaneous and is well described by the Langmuir model. The adsorption process was concluded to involve both chemisorption and physisorption through several mechanisms including electrostatic attraction, hydrogen bonding, and hydrophobic attraction. Furthermore, it was discussed that the dominance of each mechanism depends on the amount of surfactant used for CNC modification. The adsorbent has shown great stability in aqueous environment under successive dialysis cycles. In addition, the regeneration study promoted MCNC as a promising reusable adsorbent as it recovered over 85% of its original adsorption capacity after 5 cycles of sorption and desorption.

Recommendations for future work

The main objective of this research work was to investigate the mechanism of adsorption and the procedure by which CTAB contributes to the anionic dye adsorption of CNCs. In future works, investigating the effect of environmental variables, such as pH of dye solution, on the adsorption properties of MCNC and their potential in the adsorption of other anionic dyes would be of interest. Furthermore, other anionic and cationic surfactants, could be potential candidates for modifying CNCs and improving their adsorption properties.

Acknowledgments Funding was provided by the Canadian Network for Research and Innovation in Machining Technology and the Natural Sciences and Engineering Research Council of Canada.

References

- Abdul Khalil HPS, Davoudpour Y, Islam MN et al (2014) Production and modification of nanofibrillated cellulose using various mechanical processes: a review. *Carbohydr Polym* 99:649–665. <https://doi.org/10.1016/j.carbpol.2013.08.069>
- Alila S, Boufi S, Belgacem MN, Beneventi D (2005) Adsorption of a cationic surfactant onto cellulosic fibers I. Surface charge effects. *Langmuir* 21:8106–8113. <https://doi.org/10.1021/LA050367N>
- Bai L, Liu Y, Ding A et al (2019) Fabrication and characterization of thin-film composite (TFC) nanofiltration membranes incorporated with cellulose nanocrystals (CNCs) for enhanced desalination performance and dye removal. *Chem Eng J* 358:1519–1528. <https://doi.org/10.1016/J.CEJ.2018.10.147>
- Batmaz R, Mohammed N, Zaman M et al (2014) Cellulose nanocrystals as promising adsorbents for the removal of cationic dyes. *Cellulose* 21:1655–1665. <https://doi.org/10.1007/s10570-014-0168-8>
- Beyki MH, Bayat M, Shemirani F (2016) Fabrication of core-shell structured magnetic nanocellulose base polymeric ionic liquid for effective biosorption of Congo red dye. *Bioresour Technol* 218:326–334. <https://doi.org/10.1016/j.biortech.2016.06.069>
- Boczka J, Fernandes A (2017) Wastewater treatment by means of advanced oxidation processes at basic pH conditions: a review. *Chem Eng J* 320:608–633. <https://doi.org/10.1016/J.CEJ.2017.03.084>
- Chatterjee S, Chatterjee T, Lim SR, Woo SH (2011) Effect of surfactant Impregnation into chitosan hydrogel beads formed by sodium dodecyl sulfate gelation for the removal of Congo red. *Sep Sci Technol* 46:2022–2031. <https://doi.org/10.1080/01496395.2011.592520>
- Dashtian K, Ghaedi M, Shirinzadeh H et al (2018) Achieving enhanced blue-light-driven photocatalysis using nanosword-like VO₂/CuWO₄ type II n–n heterojunction. *Chem Eng J* 339:189–203. <https://doi.org/10.1016/j.cej.2018.01.107>
- Dhar N, Au D, Berry RC, Tam KC (2012) Interactions of nanocrystalline cellulose with an oppositely charged surfactant in aqueous medium. *Colloids Surfaces A Physicochem Eng Asp* 415:310–319. <https://doi.org/10.1016/J.COLSURFA.2012.09.010>
- Ding F, Gao M, Shen T et al (2018) Comparative study of organo-vermiculite, organo-montmorillonite and organo-silica nanosheets functionalized by an ether-spacer-containing Gemini surfactant: Congo red adsorption and wettability. *Chem Eng J* 349:388–396. <https://doi.org/10.1016/j.cej.2018.05.095>
- Domingues RMA, Gomes ME, Reis RL (2014) The potential of cellulose nanocrystals in tissue engineering strategies. *Biomacromol* 15:2327–2346. <https://doi.org/10.1021/bm500524s>
- Foo KY, Hameed BH (2010) Insights into the modeling of adsorption isotherm systems. *Chem Eng J* 156:2–10. <https://doi.org/10.1016/j.cej.2009.09.013>

- French AD (2014) Idealized powder diffraction patterns for cellulose polymorphs. *Cellulose* 21:885–896. <https://doi.org/10.1007/s10570-013-0030-4>
- Gao Y, Deng S, Jin X et al (2019) The construction of amorphous metal-organic cage-based solid for rapid dye adsorption and time-dependent dye separation from water. *Chem Eng J* 357:129–139. <https://doi.org/10.1016/j.cej.2018.09.124>
- Habibi Y, Lucia LA, Rojas OJ (2010) Cellulose nanocrystals: chemistry, self-assembly, and applications. *Chem Rev* 110:3479–3500. <https://doi.org/10.1021/cr900339w>
- Hu Z, Ballinger S, Pelton R, Cranston ED (2015) Surfactant-enhanced cellulose nanocrystal Pickering emulsions. *J Colloid Interface Sci* 439:139–148. <https://doi.org/10.1016/j.jcis.2014.10.034>
- Jana S, Pradhan SS, Tripathy T (2018) Poly(*N,N*-dimethylacrylamide-*co*-acrylamide) grafted hydroxyethyl cellulose hydrogel: a useful Congo red dye remover. *J Polym Environ* 26:2730–2747. <https://doi.org/10.1007/s10924-017-1168-1>
- Jin L, Li W, Xu Q, Sun Q (2015a) Amino-functionalized nanocrystalline cellulose as an adsorbent for anionic dyes. *Cellulose* 22:2443–2456. <https://doi.org/10.1007/s10570-015-0649-4>
- Jin L, Sun Q, Xu Q, Xu Y (2015b) Adsorptive removal of anionic dyes from aqueous solutions using microgel based on nanocellulose and polyvinylamine. *Bioresour Technol* 197:348–355. <https://doi.org/10.1016/J.BIORTECH.2015.08.093>
- Kaboorani A, Riedl B (2015) Surface modification of cellulose nanocrystals (CNC) by a cationic surfactant. *Ind Crops Prod* 65:45–55. <https://doi.org/10.1016/J.INDCROP.2014.11.027>
- Kargarzadeh H, Mariano M, Gopakumar D et al (2018) Advances in cellulose nanomaterials. *Cellulose* 25:2151–2189. <https://doi.org/10.1007/s10570-018-1723-5>
- Khan M, Lo IMC (2016) A holistic review of hydrogel applications in the adsorptive removal of aqueous pollutants: recent progress, challenges, and perspectives. *Water Res* 106:259–271. <https://doi.org/10.1016/j.watres.2016.10.008>
- Kumar KV, Sivanesan S (2005) Comparison of linear and non-linear method in estimating the sorption isotherm parameters for safranin onto activated carbon. *J Hazard Mater* 123:288–292. <https://doi.org/10.1016/J.JHAZMAT.2005.03.040>
- Kumari S, Mankotia D, Chauhan GS (2016) Crosslinked cellulose dialdehyde for Congo red removal from its aqueous solutions. *J Environ Chem Eng* 4:1126–1136. <https://doi.org/10.1016/j.jece.2016.01.008>
- Lin N, Huang J, Dufresne A (2012) Preparation, properties and applications of polysaccharide nanocrystals in advanced functional nanomaterials: a review. *Nanoscale* 4:3274. <https://doi.org/10.1039/c2nr30260h>
- Lin F, You Y, Yang X et al (2017) Microwave-assisted facile synthesis of TEMPO-oxidized cellulose beads with high adsorption capacity for organic dyes. *Cellulose* 24:5025–5040. <https://doi.org/10.1007/s10570-017-1473-9>
- Ling Z, Wang T, Makarem M et al (2019) Effects of ball milling on the structure of cotton cellulose. *Cellulose* 26:305–328. <https://doi.org/10.1007/s10570-018-02230-x>
- Liu S, Ding Y, Li P et al (2014) Adsorption of the anionic dye Congo red from aqueous solution onto natural zeolites modified with *N,N*-dimethyl dehydroabietylamine oxide. *Chem Eng J* 248:135–144. <https://doi.org/10.1016/j.cej.2014.03.026>
- Marco-brown JL, Guz L, Olivelli MS et al (2018) New insights on crystal violet dye adsorption on montmorillonite: kinetics and surface complexes studies. *Chem Eng J* 333:495–504. <https://doi.org/10.1016/j.cej.2017.09.172>
- Meza-Contreras JC, Manriquez-Gonzalez R, Gutiérrez-Ortega JA, Gonzalez-Garcia Y (2018) XRD and solid state ¹³C-NMR evaluation of the crystallinity enhancement of ¹³C-labeled bacterial cellulose biosynthesized by *Komagataeibacter xylinus* under different stimuli: a comparative strategy of analyses. *Carbohydr Res* 461:51–59. <https://doi.org/10.1016/j.carres.2018.03.005>
- Notley SM (2009) Direct visualization of cationic surfactant aggregates at a cellulose – water interface. *J Phys Chem B* 113:13895–13897. <https://doi.org/10.1021/jp9078234>
- Olusegun SJ, de Sousa Lima LF, Mohallem NDS (2018) Enhancement of adsorption capacity of clay through spray drying and surface modification process for wastewater treatment. *Chem Eng J* 334:1719–1728. <https://doi.org/10.1016/j.cej.2017.11.084>
- Pan Y, Wang F, Wei T et al (2016) Hydrophobic modification of bagasse cellulose fibers with cationic latex: adsorption kinetics and mechanism. *Chem Eng J* 302:33–43. <https://doi.org/10.1016/j.cej.2016.05.022>
- Penfold J, Tucker I, Petkov J, Thomas RK (2007) Surfactant adsorption onto cellulose surfaces. *Langmuir* 23:8357–8364. <https://doi.org/10.1021/LA700948K>
- Prathapan R, Thapa R, Garnier G, Tabor RF (2016) Modulating the zeta potential of cellulose nanocrystals using salts and surfactants. *Colloids Surfaces A Physicochem Eng Asp* 509:11–18. <https://doi.org/10.1016/J.COLSURFA.2016.08.075>
- Qiao H, Zhou Y, Yu F et al (2015) Effective removal of cationic dyes using carboxylate-functionalized cellulose nanocrystals. *Chemosphere* 141:297–303. <https://doi.org/10.1016/j.chemosphere.2015.07.078>
- Raeiszadeh M, Hakimian A, Shojaei A, Molavi H (2018) Nanodiamond-filled chitosan as an efficient adsorbent for anionic dye removal from aqueous solutions. *J Environ Chem Eng* 6:3283–3294. <https://doi.org/10.1016/J.JECE.2018.05.005>
- Rajeswari A, Vismaiya S, Pius A (2017) Preparation, characterization of nano ZnO-blended cellulose acetate-polyurethane membrane for photocatalytic degradation of dyes from water. *Chem Eng J* 313:928–937. <https://doi.org/10.1016/j.cej.2016.10.124>
- Ranjbar D, Hatzikiriakos SG (2020) Effect of ionic surfactants on the viscoelastic properties of chiral nematic cellulose nanocrystal suspensions. *Langmuir* 36:293–301. <https://doi.org/10.1021/acs.langmuir.9b03437>
- Salajková M, Berglund LA, Zhou Q (2012) Hydrophobic cellulose nanocrystals modified with quaternary ammonium salts. *J Mater Chem* 22:19798. <https://doi.org/10.1039/c2jm34355j>

- Shafiei Sabet S (2013) Shear rheology of cellulose nanocrystal (CNC) aqueous suspensions. <https://doi.org/10.14288/1.0165728>
- Shafiei-Sabet S, Hamad WY, Hatzikiriakos SG (2012) Rheology of nanocrystalline cellulose aqueous suspensions. *Langmuir* 28:17124–17133. <https://doi.org/10.1021/la303380v>
- Shu D, Feng F, Han H, Ma Z (2017) Prominent adsorption performance of amino-functionalized ultra-light graphene aerogel for methyl orange and amaranth. *Chem Eng J* 324:1–9. <https://doi.org/10.1016/j.cej.2017.04.136>
- Tang H, Zhou W, Zhang L (2012) Adsorption isotherms and kinetics studies of malachite green on chitin hydrogels. *J Hazard Mater* 209–210:218–225. <https://doi.org/10.1016/J.JHAZMAT.2012.01.010>
- Wang L, Wang A (2008) Adsorption properties of Congo red from aqueous solution onto surfactant-modified montmorillonite. *J Hazard Mater* 160:173–180. <https://doi.org/10.1016/j.jhazmat.2008.02.104>
- Wang Y, Zhao L, Peng H et al (2016) Removal of anionic dyes from aqueous solutions by cellulose-based adsorbents: equilibrium. *Kinet Thermodyn.* <https://doi.org/10.1021/acs.jced.6b00340>
- Wang T, He X, Li Y, Li J (2018a) Novel poly(piperazine-amide) (PA) nanofiltration membrane based poly(m-phenylene isophthalamide) (PMIA) hollow fiber substrate for treatment of dye solutions. *Chem Eng J* 351:1013–1026. <https://doi.org/10.1016/j.cej.2018.06.165>
- Wang Y, Wang H, Peng H et al (2018b) Dye adsorption from aqueous solution by cellulose/chitosan composite: equilibrium, kinetics, and thermodynamics. *Fibers Polym* 19:340–349. <https://doi.org/10.1007/s12221-018-7520-9>
- Wu Y, Luo H, Wang H et al (2013) Adsorption of hexavalent chromium from aqueous solutions by graphene modified with cetyltrimethylammonium bromide. *J Colloid Interface Sci* 394:183–191. <https://doi.org/10.1016/J.JCIS.2012.11.049>
- Wu Z, Zhong H, Yuan X et al (2014) Adsorptive removal of methylene blue by rhamnolipid-functionalized graphene oxide from wastewater. *Water Res* 67:330–344. <https://doi.org/10.1016/J.WATRES.2014.09.026>
- Xhanari K, Syverud K, Chinga-Carrasco G et al (2011) Reduction of water wettability of nanofibrillated cellulose by adsorption of cationic surfactants. *Cellulose* 18:257–270. <https://doi.org/10.1007/s10570-010-9482-y>
- Xia C, Jing Y, Jia Y et al (2011) Adsorption properties of Congo red from aqueous solution on modified hectorite: kinetic and thermodynamic studies. *Desalination* 265:81–87. <https://doi.org/10.1016/J.DESAL.2010.07.035>
- Yu X, Wei C, Ke L et al (2010) Development of organovermiculite-based adsorbent for removing anionic dye from aqueous solution. *J Hazard Mater* 180:499–507. <https://doi.org/10.1016/J.JHAZMAT.2010.04.059>
- Zaman M, Xiao H, Chibante F, Ni Y (2012) Synthesis and characterization of cationically modified nanocrystalline cellulose. *Carbohydr Polym* 89:163–170. <https://doi.org/10.1016/J.CARBPOL.2012.02.066>
- Zeng G, Fu H, Zhong H et al (2007) Co-degradation with glucose of four surfactants, CTAB, Triton X-100, SDS and Rhamnolipid, in liquid culture media and compost matrix. *Biodegradation* 18:303–310. <https://doi.org/10.1007/s10532-006-9064-8>
- Zhang SF, Yang MX, Qian LW et al (2018) Design and preparation of a cellulose-based adsorbent modified by imidazolium ionic liquid functional groups and their studies on anionic dye adsorption. *Cellulose* 25:3557–3569. <https://doi.org/10.1007/s10570-018-1815-2>
- Zhong L, Fu S, Peng X et al (2012) Colloidal stability of negatively charged cellulose nanocrystalline in aqueous systems. *Carbohydr Polym* 90:644–649. <https://doi.org/10.1016/J.CARBPOL.2012.05.091>
- Zhou Y, Hu X, Zhang M et al (2013) Preparation and characterization of modified cellulose for adsorption of Cd(II), Hg(II), and acid fuchsin from aqueous solutions. *Ind Eng Chem Res* 52:876–884. <https://doi.org/10.1021/ie301742h>
- Zhou C, Wu Q, Lei T, Negulescu II (2014) Adsorption kinetic and equilibrium studies for methylene blue dye by partially hydrolyzed polyacrylamide/cellulose nanocrystal nanocomposite hydrogels. *Chem Eng J* 251:17–24. <https://doi.org/10.1016/j.cej.2014.04.034>
- Zhu H-Y, Fu Y-Q, Jiang R et al (2011) Adsorption removal of Congo red onto magnetic cellulose/Fe₃O₄/activated carbon composite: equilibrium, kinetic and thermodynamic studies. *Chem Eng J* 173:494–502. <https://doi.org/10.1016/J.CEJ.2011.08.020>
- Zhu W, Liu L, Liao Q et al (2016) Functionalization of cellulose with hyperbranched polyethylenimine for selective dye adsorption and separation. *Cellulose* 23:3785–3797. <https://doi.org/10.1007/s10570-016-1045-4>

Publisher's Note Springer Nature remains neutral with regard to jurisdictional claims in published maps and institutional affiliations.